We are IntechOpen, the world's leading publisher of Open Access books Built by scientists, for scientists

6,900
Open access books available

185,000
International authors and editors

200M
Downloads

Our authors are among the

154
Countries delivered to

TOP 1%
most cited scientists

12.2%
Contributors from top 500 universities



WEB OF SCIENCE™

Selection of our books indexed in the Book Citation Index in Web of Science™ Core Collection (BKCI)

Interested in publishing with us?
Contact book.department@intechopen.com

Numbers displayed above are based on latest data collected.
For more information visit www.intechopen.com



Chapter

From the Laser Plume to the Laser Ceramics

Vladimir Osipov, Vyacheslav Platonov, Vladislav Shitov and Vladimir Solomonov

Abstract

The main stages of preparation of ceramic active elements of solid-state lasers are considered. The physical principles of laser synthesis of nanopowders are described. The features and processes taking place during compaction and compacts sintering are specified. Also we report on the investigation of characteristics of highly transparent ceramics on the basis of nanopowders synthesized in laser plume. It is shown that this approach enables to increase the "orange peel" formation threshold in the ceramics with strongly disordered crystalline structure. It opens the road to relatively simple synthesis technology from oxide materials and application of this ceramics as the gain media with oscillation efficiency higher than 50% and also leads to simplification of the synthesis technology of magnetoactive ceramics and to production of highly transparent YAG samples without the use of sintering heterovalent additives.

Keywords: laser plume, nanopowder, compact, sintering, highly transparent ceramics, laser ceramic elements

1. Introduction

In recent years, much attention has been paid to the developments aimed at creating solid-state lasers with a high average and peak power. This is primarily due to the wide range of applications of such laser systems: in the industry for remote cutting, welding, quenching, heat treatment and labeling of various materials [1–3], as well as in basic scientific research [4–6]. One of the key components of high power continuous and pulsed-periodic lasers is the active medium, where an inverse population of levels is created. In recent years, increasingly greater attention has been paid to the researches aimed at developing a technology to produce ceramic active elements for high-power laser systems. This is due to many advantages of optical ceramics over traditional media from single crystals and glasses: larger sizes, improved thermomechanical characteristics, the ability to synthesize composite samples, quick production, lower energy costs and price.

After pioneering work on synthesis of the laser ceramics and obtaining effective generation [7], a large amount of research was carried out in this direction. The requirements [8] are specified to achieve high-efficiency laser generation in ceramics: the thickness of the grain boundaries is of the order of 1 nm, the scattering loss per pass is less than 0.05–0.1% cm^{-1} (residual porosity at the level of 10^{-4} vol.%), optical uniformity with wavefront distortion of the λ/19.5. Using

yttrium-aluminum garnet-based ceramics ($Y_3Al_5O_{12}$, YAG) with similar characteristics in the geometry of a thin disk (active medium Ø11 × 0.15 mm), an output power of 1.8 kW with a slope efficiency of 74.1% was implemented [9]. Moreover, a record output power of 6.5 kW with a slope efficiency of 57% was achieved in [10]. In a ceramic disc 8.5% Yb:LuAG with a thickness of 0.15 mm, an output power of 1.74 kW with a slope efficiency of 71.2% was demonstrated [11]. The most impressive output power values were achieved when using active elements of a sufficiently large volume. For example, in a ceramic plate of 1% Nd:YAG with a size of 89 × 30 × 3 mm^3, the power of continuous laser generation was 2.44 kW [12], and with increasing dimensions up to 120 × 50 × 3 mm^3—4.35 kW [13]. The cascade of several Nd:YAG ceramic elements sized 100 × 100 × 20 mm^3 allowed this value to increase to 67 kW [14], and further to 105.5 kW [15].

From the point of view of energy characteristics, the impulses with an energy of 105 J for a duration of 10 ns and an average power of 1 kW at a repetition rate of 10 Hz and cryogenic cooling of a Yb:YAG/Cr:YAG element of ceramics have been implemented to date [16].

One should also note the progress in the field of implementation of ultrashort laser pulses in ceramic active media. In this direction, laser pulses of 188 fs duration [17] and 152 fs [18] were demonstrated using Yb:Y_2O_3 ceramics. The shortest duration was achieved using composite ceramic Yb:Y_2O_3/Yb:Sc_2O_3 media with a total width of the amplification band of 27.3 nm, where a record low pulse duration of 53 fs was demonstrated [19].

When developing the technology to produce ceramic active elements, the main attention is paid to the formation of a nonporous microstructure of the material while maintaining the characteristic grain size in the range from several hundred nanometers to micrometers, which is important for reducing the local depolarization of laser radiation [20]. To meet these requirements, synthesis techniques were developed based on spark plasma sintering [21–23], hot isostatic pressing [24–26], and vacuum sintering with doping of heterovalent ions [27]. The latter option is more attractive due to the less expensive and uncomplicated technology. However, this approach, with a significant content of additives (more than 1 mol.%), is fraught with a significant disadvantage due to the release of heterovalent ions during sintering into the regions adjacent to the grain boundaries. In the synthesis of oxide ceramics, the possibilities of this approach can be expanded by using nanopowders obtained by laser evaporation, where the synthesis of nanoparticles proceeds at high temperatures and rapid cooling. This will ensure high uniformity of nanoparticles and ceramics based on them.

2. Preparing nanopowders

There are many methods for preparing nanopowders: mechanical crushing, precipitation from solutions, sol-gel, self-propagating high-temperature synthesis, physical vapor deposition. However, nanopowders prepared by the method of laser evaporation of a solid target in a gas atmosphere meet the above requirements to the fullest extent possible. Indeed, the radius of such particles (5–10 nm), the range of particle size distribution is rather narrow (5–40 nm), their purity is similar to the purity of the starting material, they usually have a spherical shape. The large capillary pressure and the significant surface energy due to the large surface of such nanopowders allow, under otherwise equal conditions, to reduce the duration or the sintering temperature. However, the most important advantage of the nanopowders thus prepared is that the doping takes place directly in the laser plume at high temperature and rapid cooling. This prevents segregation of the dopants and ensures

high homogeneity of the ingredients in the nanoparticle, in the compact and, as will be shown, in samples of synthesized ceramics. In this connection, let us consider the process of laser nanopowder synthesis in more detail.

For the synthesis of oxide nanopowders by this method, a CO_2 laser (λ = 10.6 μm) and a 600 W fiber ytterbium laser (λ = 1.06 μm) were used. The average output power of the CO_2 laser was 550 W at a repetition rate of 650 Hz pulses with an energy of W = 1.4 J, a peak power of about 9 kW, and a duration of 500 μs at a power level of 0.1.

Figure 1a shows a block diagram of the laser complex for preparing nanopowders [28, 29]. Laser radiation was focused on the target with a lens, which also served as the entrance window of the evaporation chamber. The target was made from oxide micro-powder (or a mixture of them) by pressing and sintering it. As a result of the action of laser radiation, a laser plume consisting of target vapors appeared on the target near its surface. Mixing with ambient air or other buffer gas, the steam was cooled. The cooled vapor was condensed in the form of nanoparticles, which were in the evaporating chamber in a suspended state. A special drive rotated the target and moved it linearly in a horizontal plane so that the laser beam scanned the surface of the target at a constant linear velocity, thereby achieving uniform evaporation of the material from the surface. After evaporation of the surface, the target moved in a vertical direction. The fan pumped air through the chamber and transferred the powder to the cyclone and further into the electric filter where it was assembled. The air was cleaned additionally in a mechanical filter and returned to the chamber. The gas flow rate above the target surface was 15 m/s. **Figure 1b** (upper) shows photographs of the laser target before and after exposure of the CO_2 laser radiation for which the target material is opaque and the ytterbium laser radiation for which the target is semitransparent (lower). It can be seen that if the target is translucent for laser radiation, then it evaporates non-uniformly. Its surface consists of a number of needle formations 8 mm high and up to 1 mm thick.

The nanoparticles are formed in a laser plume. A laser plume is a flow of incandescent vapors of a solid target in the form of a weakly ionized plasma from the region of incidence of the laser beam on the target [30, 31]. In visible light, the plume is typically in the shape of a needle directed normal to the target surface, regardless of the angle of incidence of the laser beam (**Figure 2**). This tip is surrounded by a vortex structure, which is clearly manifested in shadow photography [32].

When exposed to single pulse or pulse-periodic laser radiation, the plume appears after the delay time td. During this time, the target substance is heated to

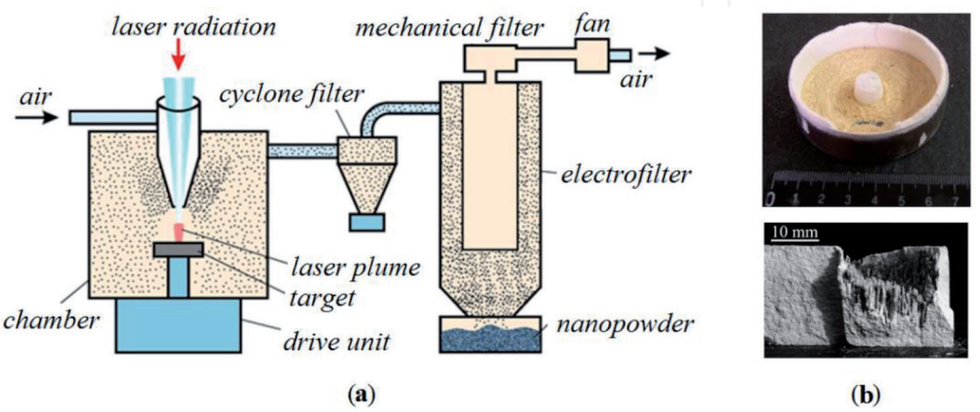


Figure 1.
Preparing a nanopowder: (a) block diagram of the laser complex for preparing a nanopowder, (b) image of laser target after exposure to radiation CO_2 laser (top), ytterbium fiber laser (bottom) [29].

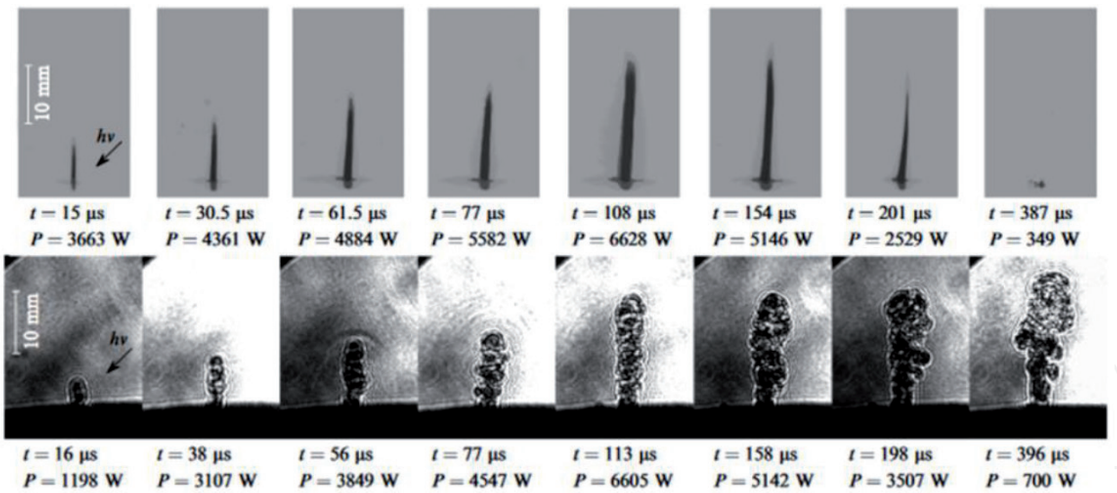


Figure 2.
Scanning of photographs (exposure 1 μs) of a laser plume (CO_2 laser pulse duration 200 μs, incident angle of 45°). Top row: visible light photography, bottom row: shadow photography. The captions below them indicate the shooting delay time relative to the start of the plume initiation (t) and the peak laser power (P) at the time of shooting [30].

the evaporation temperature in the area of the laser beam incidence. For a linear leading edge of a laser pulse, the delay time is defined as td = $2W_d/P_d$. Here, W_d is the energy required for preheating the target substance to the evaporation temperature, and P_d is the instantaneous power of laser radiation at the moment of the flare appearance. For different substances, due to the difference in W_d, the delay times of t_d differ. After the appearance of the glow (l = 0), the height of the plume (l) increases at a rate proportional to the square root of the peak power of the laser pulse. The maximum height of the plume (l_m) is reached at the moment of the maximum laser pulse. The diameter of the luminous zone of the plume is typically 0.5–1.0 mm, which approximately corresponds to the size of the laser spot on the target surface.

Over the entire length of the plume, its emission spectrum is represented by dominated structured molecular bands of radicals of cations of the target substance [31] against the background of a continuous band of recombination radiation (**Figure 3**). In this case, the short-wave part of the spectrum is well approximated by the Wien's curve, which makes it possible to determine the temperature of

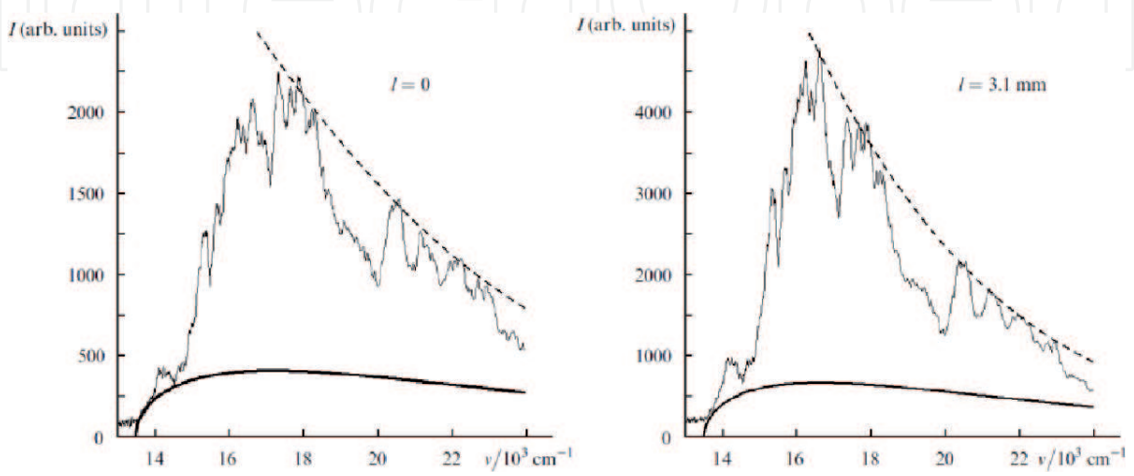


Figure 3.
The spectrum of the plume glow from a CO_2 laser at different distances (l) from the target of yttrium-stabilized zirconium oxide (solid curve), recombination radiation (bold curve), and approximation of the Wien's curve (dashed line) [31].

the luminous gas in the flare. Thus, when irradiated with a pulsed CO_2 laser, the maximum temperature close to the boiling point of the target material is reached at the target surface, and the flame temperature decreases nonmonotonically as it moves away from the target. When irradiated with pulses of a fiber ytterbium laser (1.07 μm), the temperature of the plume near the target slightly exceeds the melting point of the substance.

The transverse dimensions of the crater that appears on the target after exposure to a laser pulse almost coincide with the size of the laser spot on the target, and its depth depends on the wavelength of the laser radiation. For example, at the same pulse energy (1.0–1.4 J) after CO_2 laser irradiation, the crater depth is 5–10 μm, almost independently of the target substance. After a fiber laser pulse, the crater depth is 6–8 times greater, and with repeated exposure, the target surface becomes needle-like. These features are due to different mechanisms of absorption of radiation by the target of these. Thus, the frequency of a photon at the wavelength of a CO_2 laser is comparable to the frequency of optical phonons of oxide crystals. Therefore, in this case, such materials are almost opaque and the depth of penetration of laser radiation into them is only a few micrometers. For fiber ytterbium laser radiation, oxides we used are transparent – absorption is possible only on crystal and mechanical defects of the target. If these materials are single crystals with a minimum content of defects, the characteristic depth of penetration of laser radiation into them is tens of centimeters. This corresponds to the absorption index $\alpha \sim 10^{-2}$–$10^{-3} cm^{-1}$. If such defects are located inside the target in the area of the laser beam incidence, the initial heating also occurs inside the target (in the area of these defects). Then, due to the strong temperature dependence of the absorption coefficient, a heat wave is formed [33], which moves along the laser beam from the defect to the target surface, upon reaching which a laser plume is formed. This process is compounded by the fact that after repeated exposure, the surface of the initial target is covered with a layer of transparent melt 100–400 μm thick, in which the defect concentration is much lower than in the initial target made of sintered micro-powder.

This model is confirmed by the fact that the delay time for the appearance of a laser flare from the beginning of the laser pulse exposure has a large spread and on average increases with increasing transparency of the target. In particular, the delay in the appearance of a laser plume on the surface of a semitransparent Nd:Y_2O_3 ceramic with $\alpha = 23\ cm^{-1}$ (an analog of the fused layer) averaged over several radiation pulses was 5–10 times greater than for the original sintered micro-powder target ($\alpha = 1.7 \times 10^3\ cm^{-1}$) at the same radiation intensity $I = 0.4\ MW/cm^2$ [31]. The spread of the delay in the formation of a laser plume during evaporation of the same target is due to the stochastic nature of the depth of defects from the target surface at different points.

When nanopowders are obtained using both lasers, in addition to nanoparticles, spherical particles with sizes from 0.5 to 150 μm are also formed [29, 33], as well as shapeless target fragments of the same size. Fragments are formed after the end of radiation exposure to a specific part of the target due to thermal splitting of the cooling fused layer [30]. Spherical particles are liquid droplets of the melt, is sprayed by the vapor pressure of the laser crater.

Especially many drops are formed when the target is vaporized by continuous ytterbium laser radiation. At the same average radiation power (600 W) and the same intensity on the target as for the CO_2 laser ($\approx 1.3\ MW/cm^2$), the production capacity of the Nd:Y_2O_3 nanopowder decreased to 15 g/h, and its output during evaporation of one target to 9 wt.% [34]. High-speed shooting of the laser plume showed that this effect is due to the transition from steam to vapor-drop ablation. The latter becomes dominant ~500 μm after the start of the laser pulse. A similar

pattern is observed in the evaporation of targets from YSZ and $FeMgAl_2O_4$. Theoretical analysis [33] allowed us to establish that one of the reasons for the appearance of drops in the laser flare is related to the presence of melt in the crater and is due to the development of the Kelvin-Helmholtz instability that is formed between the liquid wall of the crater and the flow of expiring vapor. This analysis made it possible to establish the characteristic size of the instability:

$$\lambda_e = \frac{2\pi\sigma}{\rho_2 V^2} = (20 \div 90) \cdot 10^{-6}\,\text{m} \quad (1)$$

and its development the increment

$$\tau = \frac{3\sqrt{3}\pi\sigma}{\rho_2 V^3}\sqrt{\frac{\rho_2}{\rho_1}} \approx 100\ \ \mu s, \quad (2)$$

where ρ_1 and ρ_2 are the melt and vapor densities, σ is the surface tension coefficient, V is the vapor flow rate.

Optimizing the duration (<00 μs) and radiation density, separation and trapping, it was possible to prepare high-quality nanopowders. **Figure 4** shows an example of a photo of YSZ nanopowder, and the distribution of particles of different composition in size is given as an example. Depending on the thermophysical properties of refractory oxides, the pressure and speed of the carrier gas, the productivity of producing a nanopowder using a CO_2 laser with an average radiation power of 600 W varies from 10 to 80 g/hour.

The distinguishing feature of nanoparticles synthesized in a laser plume, i.e. at a high temperature and rapid cooling, is a high homogeneity of the distribution of components in the volume. This is confirmed by the results of a study of the distribution of the concentration of dopant (Yb) in the Lu_2O_3 matrix, carried out in the scanning electron microscope (SEM) mode using the X-ray spectral microanalysis (X-ray SMA) method. The results of mapping the elemental composition of individual nanoparticles are shown in **Figure 5**. It follows from these images that the dopant is distributed uniformly over the Lu_2O_3 matrix, and there is no increased Yb concentration on the particle surface.

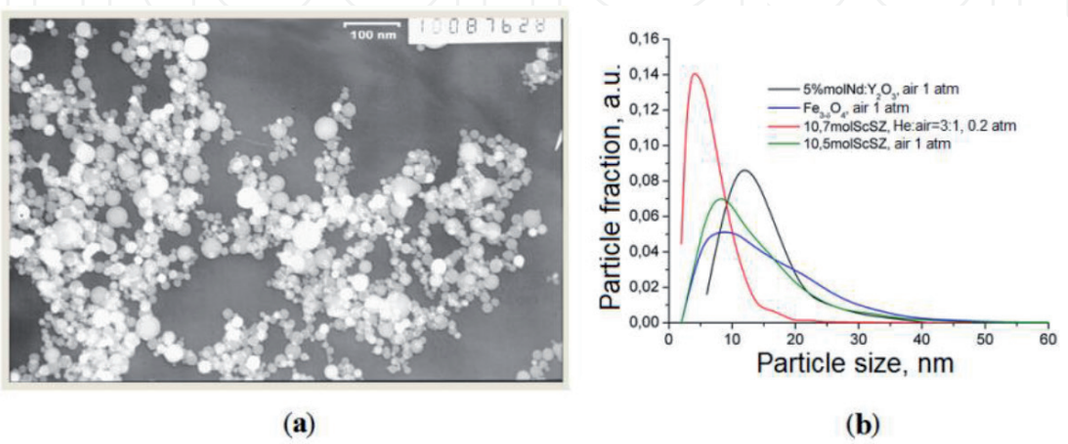


Figure 4.
A typical photo of YSZ nanoparticles (a) and the size distribution of nanoparticles of different compositions (b) [29].

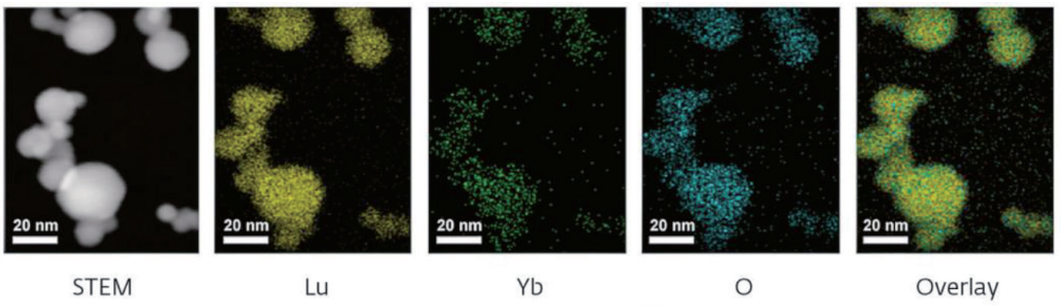


Figure 5.
Results of mapping the elemental composition of Yb:Lu_2O_3 nanoparticles with the use of SEM and X-ray SMA.

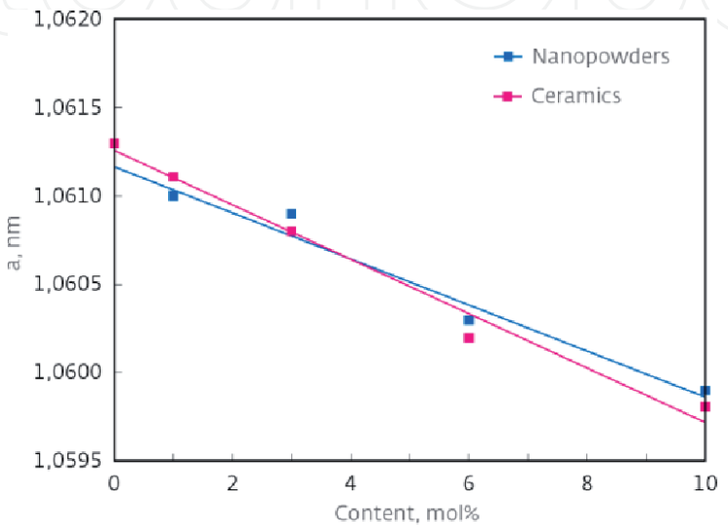


Figure 6.
Results of X-ray diffraction analysis of ceramics and nanopowders with different concentrations of HfO_2 [35].

This finding is supported by the results of X-ray diffraction analysis of Nd:Y_2O_3 nanopowders and ceramics doped with HfO_2 (**Figure 6**). It can be seen that the dependence of the parameters of the crystal lattice on the HfO_2 content is linear. This indirectly indicates a homogeneous occurrence of Hf in a Y_2O_3 matrix and the absence of second phases, both in a nanopowder and in ceramics.

A feature of the above method for producing nanopowders is that they crystallize in a laser plume, as a rule, in metastable phases. For example, yttrium oxide nanopowders crystallize in the monoclinic phase, while alumina nanopowders in the γ-phase. This effect is associated with very rapid cooling and quenching (within ≈1 ms) of the resulting nanoparticles during vortex mixing of the laser plume with air and, possibly, with the resulting oxygen deficiency in nanoparticles formed from trivalent cation radicals.

3. Compacting, annealing and sintering of nanopowders

The requirements that are imposed on the methods of "cold" pressing are, first of all, maximally possible compact density and uniformity of stacking of powders. To produce highly transparent ceramics, the following compacting methods are most often used: slip casting, slip casting under pressure, cold isostatic pressing, static pressing, static pressing with ultrasonic treatment on nanoparticles, magnetic pulse compacting.

In [36], the transparency of laser ceramics was investigated using compacts prepared by slip casting and dry pressing. It was shown that ceramics samples, whose

compacts were prepared by cold isostatic pressing, have greater transparency than with slip casting. This difference is attributed to the high viscosity of the slip using nanoparticles, which prevented tight packaging. At the same time, when using hot pressing at 1750 °C and a pressure of 200 MPa, the samples prepared by slip casting have better characteristics than those based on the compacting of dry powders. However, the use of hot pressing is a complex and expensive step, therefore, there is a strong desire to create a technological chain of preparation of samples with theoretical transparency, without the use of hot pressing.

Given the above, the most studies are conducted using dry cold pressing of nanopowders. For these purposes, we have tested the method of static pressing of nanoparticles with and without ultrasonic treatment (UST), magnetic-pulse pressing and cold isostatic pressing. All of them showed rather close relative densities of compacts at the same pressures, which is confirmed by the results presented in [36, 37]. Nominally pure and neodymium-activated yttrium oxide nanopowders, designated by us as Y_2O_3, 8 NDY, 3NDY, and 1NDY (the number before the letter symbol NDY denotes the content of neodymium oxide in mole percent in nanopowder) were used in the experiments. For comparison, the dry nanopowders (without plasticizers) of all these types were pressed as uniaxial static pressing (without UST), and under the influence of ultrasonic vibrations. The pressures were 240, 480, and 720 MPa. The diameter of the pressed samples was 14 mm, the height of the samples was 2–4 mm. The experimental results in the form of the dependence of the relative density on the compacting pressure at a constant power of UST 3 kW and 0 kW (i.e. without UST) are shown in **Figure 7**.

According to the technique described in [37], the parameters of the pressing equation *b* and *Pcr* for each type of nanopowder were determined from the experimental compaction curve. The compression curves of the samples were described by the logarithmic compression equation in dimensionless form:

$$\rho / \rho_{theor}(P) = b \cdot Ln\left(\frac{P}{P_{cr}}\right) + 1 \qquad (3)$$

where ρ is the density of the compact, ρ_{theor} is the theoretical density, b is the compaction rate, P_{cr} is the design pressure at which the theoretical density is reached. The results obtained show that the relative density of the compacts of the studied nanopowders is slightly dependent on the UST and is determined mainly by the compacting pressure, thereby confirming the findings obtained using other methods.

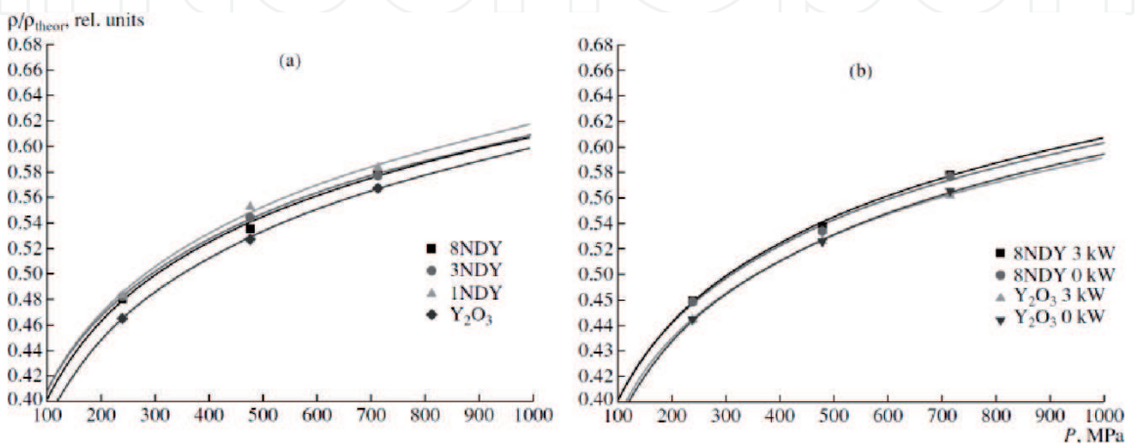


Figure 7.
Curves of nanopowder compaction: (a) 8NDY, 3NDY, 1NDY, Y_2O_3 with UST, W = 3 kW; (b) 8NDY, Y_2O_3 with UST W = 3 kW and without UST (W = 0 kW) [37].

The effect of nanoparticle size on compacts density is discussed in [38] using the above method, the granular dynamics. The calculations were carried out for nanopowders with particle sizes from 10 to 100 nm. Typically, deterioration of compressibility with decreasing particle sizes is associated with adhesion of the individual particles, which results in the formation of strong aggregates. As possible causes of the size effect are called Van der Waals forces of attraction, the absence of plastic deformation of nanoparticles, the formation of chemical bonds, electrostatic interaction, etc. The authors [38] sought to take into account the most important of these reasons. Their calculations of the dependence of the density of compacts on the axial pressure are shown in **Figure 8**.

Under the initial anisotropic configuration, the distribution of particles with the presence of vertical chains and a coordination number exactly equal to two accurately was adopted. It can be seen that as the particle size increases at the same pressing pressures, the density of the compacts increases substantially. We should also pay attention to the important role that the Van der Waals forces create (curve 4). Of course, there is no exact agreement with the experimental data, but the trend can be traced unequivocally. This fact raises the question of which nanopowders are most preferable for the synthesis of laser ceramics. On the one hand, small particles due to high surface energy provide high sinterability, and in the case of nanopowders, produced by laser evaporation, - greater solubility of ingredients in each other and particle uniformity, but poorer compressibility. This question remains open in relation to the synthesis of laser ceramics up to this point. Further, the results obtained using a nanopowder, obtained by laser evaporation of a solid target, with an average particle size of 10–20 nm and uniaxial static pressing will be presented for the preparation of compacts with dimensions less than 30 mm. Cold isostatic pressing was used for compacts of larger diameter. The prepared compacts with a relative density of 0.46–0.58 are usually air calcined to remove organic matter and to provide additional oxidation and phase transformations.

Figure 9 shows the dependence of the grain size on the calcination temperature. Each point on the graph corresponds to its own pattern. It can be seen that the grain sizes grow reasonably from 24 to 77 nm with an increase in temperature from 715 °C to 1300 °C, and the last point, apparently, is caused by a measurement error.

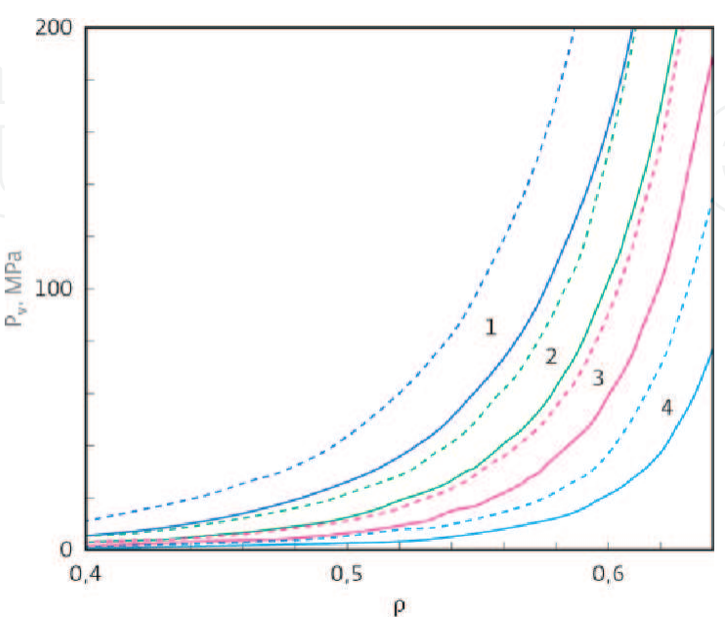


Figure 8.
Axial pressure as a function of the compact density for systems with a particle size d = 10 nm (1), 30 nm (2), 100 nm (3) and a system without Van der Waals forces (4). Solid lines are isotropic initial configurations; dashed lines are anisotropic configurations [38].

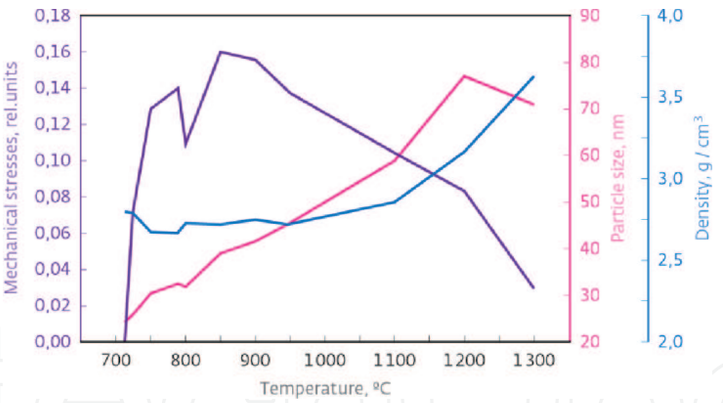


Figure 9.
Dependence of the grain size, mechanical stresses and densities of compacts on the calcination temperature of compacts from the nanopowder of the monoclinic phase [35].

The dependence of the mechanical stresses and density of compacts on temperature is also given there: after transformation at 715 °C into a cubic phase which parameters are greater than in the monoclinic one, mechanical stresses increase with the temperature raise, followed by a certain decrease, accompanied simultaneously by a shock of condensation of compacts, that we also interpreted as a mechanical ordering of grains. Further, the behavior of the curves is logical: the density of compacts increases, mechanical stresses decrease.

Sintering can be conditionally divided into three stages. The dependencies shown in **Figure 9**, characterize the processes in two of the three stages of sintering. In stage I (700–1200 °C), there is no shrinkage of the compact, but mass transfer from convex to concave surfaces occurs, mainly by near-surface diffusion. This leads to a decrease in the free surface of nanoparticles, which means that they smooth out, spheroidize and increase the size of contact spots between nanoparticles. In the case of nanopowders, the latter process leads to an increase in the dimensions of the nanoparticles, which is not observed for particles with dimensions of ~1 μm.

After 1200°C, a second stage is observed, characterized by rapid shrinkage of the sample. This is due to the diffusion sliding of the grains and the diffusion adjustment of their shape, as well as the "evaporation" of vacancies from the pore surface in the bulk of the particles, with their subsequent exit to the crystallite boundaries and displacement in the boundary layer. Since the particle sizes in our case are small, there are many grain boundaries, then the shrinkage process occurs quite intensively.

When the compacts are compacted, the diffusion processes are decisive. Therefore, an increase in these rates by introducing hetero- and isovalent additives that form solid solutions can significantly accelerate the compaction. In this case, heterovalent additives lead to the formation of vacancies that are much higher than their thermodynamic content in the unalloyed matrix. The introduction of isovalent additives leads to lattice distortion. Both these additives lead to an acceleration of mass transfer, release and filling of pores. When sintering with such additives, a situation may occur where the removal of pores outstrips the growth of crystallites. In this case, these processes are separated, and the crystallites grow non-porous, which facilitates the synthesis of high-transparency ceramics. Moreover, the introduction of additives changes the conditions for the transition of an atom across the boundary, which can significantly affect the final dimensions of the crystallites. We have investigated the replacement of the Y^{3+} cation in Nd^{3+}:Y_2O_3 with isovalent ions Lu^{3+} or Sc^{3+} ions or the Zr^{4+} and Hf^{4+} heterovalent ions, and also the Al^{4+} cations by Ce^{3+} in garnet ceramics. The compacts with a diameter of 15–32 mm, a thickness

of 0.5–3.5 mm with a relative density of ~0.5 were sintered. The parameters of sintering varied over a wide range: the sintering temperature T = 1550–2050°C; sintering time t_s = 1–30 h; the rate of temperature rise v_T = 0.75 and 5.0 K/min. The influence of these factors on the characteristics of high-transparency ceramics will be discussed in the next section.

4. Highly transparent ceramics for lasers

Highly transparent ceramics are more commonly used as active elements of solid-state lasers intended for various purposes, optical armor, scintillation sensors, heat and mechanically resistant windows, bulbs for high-power high-pressure lamps, wide-angle lenses, etc. It was previously noted that ceramic samples of the highest optical quality are usually obtained using hot isostatic pressing. This is a rather expensive and complex technology. Therefore, numerous studies are being conducted to find technological solutions to avoid this operation. Here we present the results of only one of the ways to solve this problem, which is related to the use of nanopowders with a small average particle size and high uniformity of their composition within each of the nanoparticles. Let's consider the characteristics of a number of ceramics for various purposes prepared using nanopowders synthesized in a laser plume.

4.1 Ceramics with disordered crystalline structure

Such ceramics are formed by replacing matrix cations with impurity cations. This leads to a change in the local crystalline fields in the positions of the activator ions and, therefore, to broadening of the spectral lines and the gain band.

First the focused broadening of the laser transition band was implemented in ceramic yttrium-aluminum garnet [39], when a part of aluminum ions was replaced by scandium ions, i.e. ion of the same valence. In this ceramic, activated by Nd^{3+}, a laser pulse with a duration of 10 ps was obtained on its optical transitions in the 1 μm region, and when the neodymium was changed to ytterbium, it was reduced to 96 fs [40].

At the same time, it was found that the greatest broadening of the gain band is achieved in the ceramics based on yttrium oxide with the introduction of heterovalent ions. However, in [41] the doping with such ions did not allow achieving the transparency necessary for high-performance generation [35]. According to the authors, this was prevented by the formation of an "orange peel" due to the increased concentration of dopants near the intercrystalline boundaries. Since this class ceramic is important for the development of laser technology, we investigated its creation using two approaches. In the first case, the traditional approach [7] was implemented, i.e. the ceramics were synthesized from nanopowders of simple oxides Yb_2O_3, Nd_2O_3, Y_2O_3, HfO_2 and ZrO_2, mixed in the required ratio. We refer to them as to "mixed" powders. The second approach is original [42] and consists in the fact that the necessary components were mixed in the preparation of a laser target, and the synthesis of nanoparticles occurred in a laser plume, i.e. at high temperature and rapid (<1 ms) cooling. Let's refer to these powders as to "laser" ones.

Using these approaches, the samples of ceramics based on yttrium oxide with HfO_2 or ZrO_2 additives were prepared. The samples were 2–3 mm thick and 11 mm in diameter. Analysis of the appearance of the ceramics' samples based on yttrium oxide, obtained by different approaches, shows that they differ insignificantly. The differences are manifested in the study of their light scattering. **Figure 10** shows photographs of the initial radiation of the laser (λ = 633 nm) incident on the screen and of the radiation passing through samples of "mixed" and "laser" powders

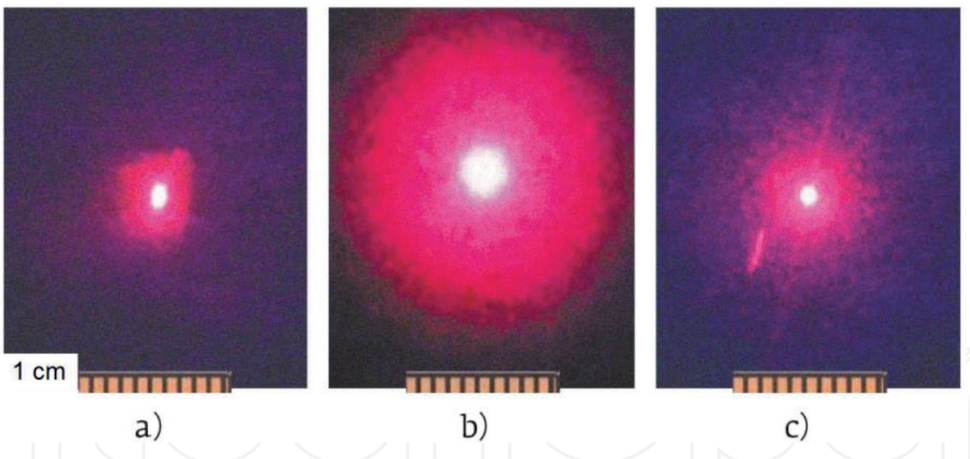


Figure 10.
The initial radiation of a semiconductor laser (λ = 633 nm) incident on the screen (a) and the radiation transmitted through the ceramic samples [(YbxLuyY1−x−y)$_2$O$_3$]1−z(ZrO$_2$)z from the "mixed" (b) and laser (c) powders [42].

having the same chemical composition $[(Yb_xLu_yY_{1-x-y})_2O_3]_{1-z}(ZrO_2)_z$. It can be seen that the ceramic made of "mixed" powders possesses a large light scattering and transparency by 15–20% lower than that made of laser powders [42], therefore it is not yet suitable for obtaining high-performance generation.

In this connection, the ceramics prepared from "laser" powders were investigated further. Their disordered crystalline structure manifests itself in the broadening of the emission bands at laser transitions between the Stark levels of the neodymium ion $^4F_{3/2} \leftrightarrow {}^4I_{11/2}$ and of the Yb^{3+} ion $^2F_{5/2} \leftrightarrow 2F_{7/2}$ (**Figure 11**). Moreover, it was found that the additives lead to a complete overlap (at a level less than 0.4 of the maximum intensity) of the contours of the two neodymium emission bands at λ = 1060 nm and 1075 nm (**Figure 11**, left). This leads to the formation of a continuous emission band with a width of up to 50 nm (on the base) in the range of 1040–1090 nm [42].

In the optical ceramics activated with ytterbium, the above additives also lead to broadening of the luminescence bands at λ = 1030 and 1075 nm on a laser transition between the Stark levels of the Yb^{3+} ion $^2F_{5/2} \leftrightarrow {}^2F_{7/2}$ (**Figure 11**, right). A complete overlap of the bands is observed at a minimum level of 0.25 of the maximum intensity with the width of the continuous band at this level reaching 100 nm on the base [42, 43].

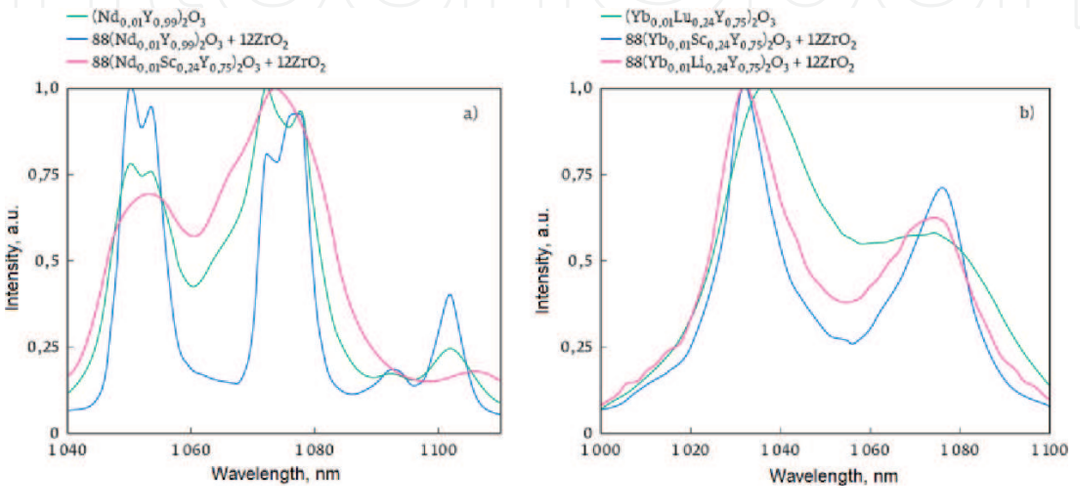


Figure 11.
IR spectra of luminescence of ceramic samples activated with Nd^{3+} ions (left) and Yb^{3+} ions (right) [42].

In the ceramics with additions of zirconium and hafnium, the trivalent Hf^{3+} and Zr^{3+} ions were found [42–44], which is confirmed by electron paramagnetic resonance spectra [44]. In the crystal, $3d^{10}4d^1$ Zr^{3+} and $4f^{14}5d^1$ Hf^{3+} ions form two Stark levels: the orbital doublet (E) and the triplet (T_2), with the energy gap equal to the strength of the crystal field in the positions of these ions. In yttrium oxide, these ions replace yttrium ions in two positions C_2 and C_{3i}, differing in symmetry and the strength of the crystalline field. Therefore, in the pulsed cathodoluminescence spectra of the ceramics containing zirconium or hafnium, both ions (Hf^{3+} and Zr^{3+}) emit two bands each, at λ = 818 nm and 900 nm about 30 nm wide [42, 43]. Furthermore, the energy of the radiative level of the short-wave band (12225 cm^{-1}) of the Hf^{3+} and Zr^{3+} ions coincides with the energy of the pumping level of $^4F_{5/2}$ (12138–12436 cm^{-1}) of the neodymium ion, and the energy of the radiative level of the second longer wavelength band (11100 cm^{-1}) – with that of the upper laser level $^4F_{3/2}$ (11208–11404 cm^{-1}) of the Nd^{3+} ion. It is because of the negative influence of the Hf^{3+} and Zr^{3+} ions on the inverse population of the laser levels caused by this coincidence, that we have not obtained laser generation on the neodymium ion ransitions in the ceramics with disordered crystalline structure with additions of hafnium or zirconium.

Another situation is observed for the activator Yb^{3+} ion. The energy of its upper laser level $^2F_{5/2}$ (10240–10673 cm^{-1}) is less than the energy of the radiative levels of Hf^{3+} and Zr^{3+} ions. Therefore, the Hf^{3+} and Zr^{3+} ions do not affect the population of the $^2F_{5/2}$ level of the Yb^{3+} ion, which allowed generation of laser radiation in disordered ceramic consisting of $0.88[(Yb_{0.01}Lu_{0.24}Y_{0.75})_2O_3]+0.12ZrO_2$ [42] obtained from "laser" nanopowders of a solid solution. The generation properties were investigated in a three-mirror V-shaped resonator formed by two spherical mirrors with radii of curvature of 100 mm and an output plane mirror with a transmittance of 1.2, 2.4 and 5.0%. The active element in the form of a polished ceramic disk 1.27 mm thick was installed in the resonator between spherical mirrors at the Brewster angle. Pumping was carried out through a dichroic spherical mirror with a reflection coefficient of 99.9% in the range of 1020–1100 nm and a transmittance factor of 98% in the range of 950–980 nm by a laser diode radiation with a fiber output of 9 W at a wavelength of 975 nm and a bandwidth of 3 nm. With an output mirror with a transmittance factor of 1.2, 2.4 and 5.0%, the slope efficiency was 16.5, 26.0 and 29.0% with an optical efficiency of 6.8, 7.0 and 9.5%, respectively.

Relatively low values of the laser generation parameters obtained are due to the presence of an "orange peel" in the ceramics with a high content (12 mol%) of zirconium. In the ceramic consisting of $0.95[(Yb_{0.05}Lu_{0.15}Y_{0.80})_2O_3] + 0.05ZrO_2$ with a content of the sintering additive ZrO_2 reduced to 5 mol%, the "orange peel" is not clearly manifested. While investigating the generation properties [45], it was found that the laser generation band on this ceramic (**Figure 12**) practically coincides with the IR-luminescence band (**Figure 11**, right), its width reaches 97 nm at the base, which is currently a record value in the visible and near-IR wavelengths. On this entire band, quasi-continuous generation with a slope efficiency equal to 49.3% and 51.2% in the band maxima at the wavelengths of 1077 and 1032 nm, respectively, was obtained. These factors provide good prospects for the development of lasers with ultrashort pulses and lasers with a wide range of smooth frequency tuning.

4.2 Ceramics of yttrium-aluminum garnet

Taking into account the importance for the creation of technological lasers and high-scale laser systems, the great attention has been paid to YAG ceramics, doped with Nd or Yb. Extensive studies have been carried out, the results of which have been presented in a number of reviews, for example [46], and monographs [8],

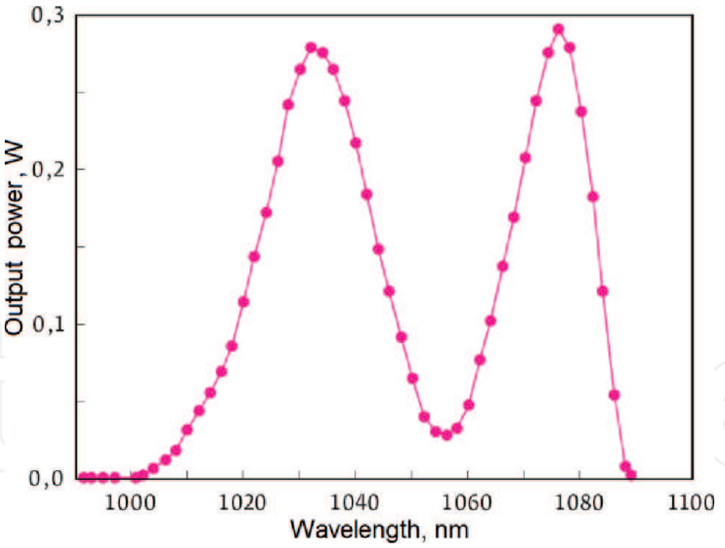


Figure 12.
Laser generation band of 0.95[$(Yb_{0.05}Lu_{0.15}Y_{0.80})_2O_3$] + 0.05$ZrO_2$ ceramics [45].

the methods for obtaining nanopowders, compaction and sintering have been developed that make it possible to synthesize samples with a transparency close to the theoretical one [8] and to generate a radiation with an efficiency of more than 74%. High-level results were obtained using both hot isostatic pressing (HIP) and vacuum sintering, but the presence of sintering additives in a mixture of nanopowders as TEOS [7] and MgO [47] was always mandatory. Using the nanopowders prepared by the laser synthesis method, we have studied the feasibility of synthesizing YAG ceramics without the use of these additives. Various approaches to the preparation of nanopowders were involved.

The successful attempt to produce highly transparent YAG ceramics without the use of sintering additives was associated with the mixing of separately obtained Nd:Y_2O_3 and Al_2O_3 nanopowders in the ratio of 3/5. Measured by the BET method the specific surface area of the Nd:Y_2O_3 powder was 50.7 m^2/g. It was a solid solution based on monoclinic yttrium oxide with crystalline lattice parameters a = 13.92 Å, b = 3.494 Å, c = 8.611 Å, β = 101.2°. After calcination at a temperature of 1000 °C for 30 minutes, the surface area of the powder was 25 m^2/g for conversion to the cubic phase, i. e. the particle size increased from 12 to 49 nm. Al_2O_3 nanopowder was also obtained by laser evaporation of a target followed by condensation of vapors in the air stream. Its specific surface, was 109.67 m^2/g. X-ray fluorescence analysis showed that the powder consists mainly of the γ-Al_2O_3 phase and the δ-phase content was less than 10%.

These powders were mixed in the indicated proportion in a drum mixer with an inclined rotation axis for 24 hours. Further, briquettes with a density of 20% compared to the theoretical were compacted from this mixture, which were then calcined at 1200 °C for 3 hours. As shown by X-ray fluorescence analysis, the YAG phase content in the briquettes was 96–98%. These briquettes were then milled by YSZ balls in a planetary mill for 48 hours.

The analysis of powder images after grinding showed that the agglomerates of the particles formed after calcination had an average size slightly less than 1 μm, but sometimes their size was close to 10 μm. The compacting of nanopowders into disks with a diameter of 15 mm and a thickness of 1.5–4.5 mm was carried out by the method of dry uniaxial static pressing without the use of any additives. The compacting pressure in these experiments was unchanged and was 200 MPa, which made it possible to obtain a density of 61.8%. Sintering was performed at a temperature of 1760 °C for 20 hours. The pore content in the samples was ~60 ppm, and the

transparency was 83.28%. For the first time in the Nd: YAG ceramics that did not contain sintering additives, the generation was obtained with an average power of up to 4 W and a slope efficiency of 19% [48]. However, much better results were achieved when 0.5 wt% TEOS sintering additive was added to the nanopowder. In this case, the slightly agglomerated Nd:Y_2O_3 and Al_2O_3 nanoparticles of spherical shape with dimensions of 8–14 nm were calcined at a temperature of 900–1200 °C for transformation from the monoclinic to the cubic phase. These calcined nanopowders were weighed to ensure the $Nd_{0.03}Y_{2.97}Al_5O_{12}$ stoichiometry and mixed in a ball mill with an inclined axis of rotation in alcohol with the addition of 0.5 wt% TEOS for 48 hours.

Using the previously described approach, Nd(Yb):YAG ceramic samples were synthesized. **Figure 13** shows a photograph of a Nd:YAG ceramic sample, its transmission spectrum, and also the transmission spectrum of a single-crystal laser of the same composition, which has theoretical transparency. It can be seen that in the wavelength range of more than 450 nm, these spectra practically coincide. Compared with the above results, the optical quality of the resulting ceramic due to the presence of SiO_2 was improved due to a partial reduction in agglomeration of the powder during the calcination step, inhibition of crystallite growth and pore removal due to the formation of the liquid phase, which led to reducing their content to 17 ppm. Similar results were obtained by compacting the calcined Nd:Y_2O_3 and Al_2O_3 nanopowders into compacts with a relative density of 48% and reactive sintering at 1780 °C for 20 hours.

The comparative studies of our samples and samples by Konoshima Chemical [50] were carried out jointly with the National Institute of Optics (Florence, Italy). They had the same composition (1 at.% Nd:YAG) and a thickness of 1.5 mm. To obtain the generation, a V-shaped resonator was used (**Figure 14a**). Pumping was carried out through an end dichroic mirror having high transparency for pumping radiation and high reflection for the generated radiation and spaced from the sample by 4 mm. The distance from the end EM and the output mirror OC to the rotary mirror FM was 280 mm. The OC transmission varied between 2–20%. Pumping was carried out by rectangular pulses of a duration of 10 ms and a frequency of 12.5 Hz. Their peak power was 32 W, the radiation focusing spot was 0.8 mm.

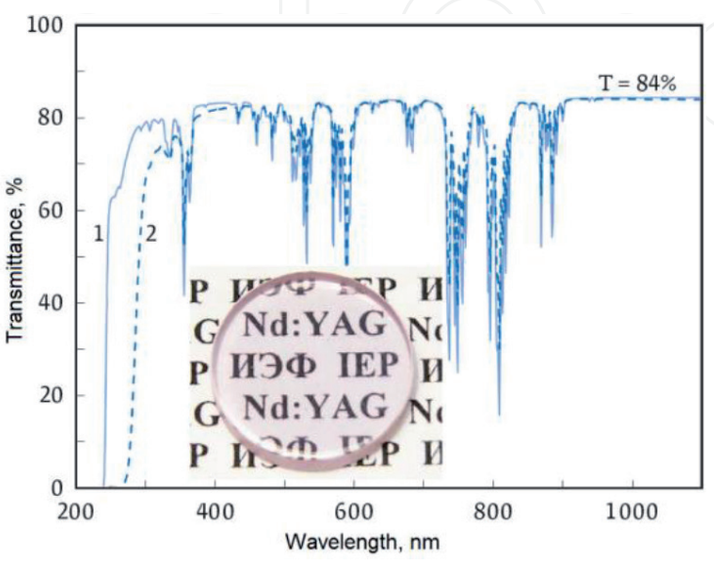


Figure 13.
Transmission spectra of Nd:YAG single crystal (1) and ceramics (2). The inset shows a photograph of ceramics [49].

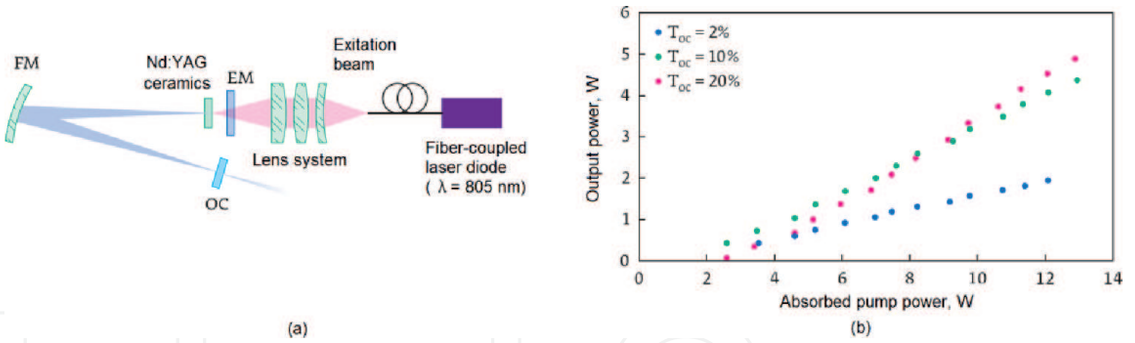


Figure 14.
Flow-chart of the experimental setting (a) and the dependence of the generation power on the pump power (b) [50].

	T_{oc} = 20%		T_{oc} = 10%		T_{oc} = 2%	
	P_{out}, W	η_S, %	P_{out}, W	η_S, %	P_{out}, W	η_S, %
IEP UrB RAS	4.91	52.7	4.38	35.5	2.07	16.7
Konoshima Chemical	5.29	53	4.69	40.4	2.49	16.6

Table 1.
Laser characteristics of Nd:YAG ceramics [50].

The dependence of the output power on the pump power is shown in **Figure 14b**. Similar results were obtained for the samples of Konoshima Chemical. Comparative data are given in **Table 1**. The best results were obtained with a transparency of the output mirror T_{oc} = 20%, when the radiation power was P_{out} = 4.91 W, and the slope efficiency η_{sl} = 52.7%. Thus, the introduction of a sintering additive in the form of TEOS had a significant effect on improving the characteristics of samples prepared from nanoparticles synthesized in a laser plume.

5. Conclusion

The main stages and processes taking place in the preparation of high-transparent ceramics, including laser ones. The optimal conditions at which the productivity of nanopowder production is realized, depending on the thermophysical properties of the material, were found to be 10–80 g/h. It is shown that the nanoparticles obtained are weakly agglomerated, have a spherical shape and an average size of ~10 nm. A feature of such nanoparticles is the high homogeneity of the composition at a high level of doping. It is shown that the density of compacts does not depend on the method of dry pressing and is determined by pressure, although the level of residual mechanical stresses differs. Pressing was carried out at diapason of pressures of 250–300 MPa, at which compact densities were ~50%.

The use of nanopowders synthesized in a laser plume for the preparation of highly transparent ceramics makes it possible to increase the threshold for the formation of an "orange peel". This opens the road to the use of sesquioxides with highly disordered crystalline structure as active elements of solid-state lasers using a relatively simple technology. In particular, this approach allowed to obtain the following.

1. In samples based on Y_2O_3 doped with Yb_2O_3 and ZrO_2, the slope efficiency of radiation generation can exceed 50%, and the band for smooth tuning of the radiation frequency can reach 100 nm.

2. Highly transparent YAG samples are prepared without the use of sintering additives, where the transparency and generation efficiency, however, is inferior to those realized when doping TEOS.

Acknowledgements

The research was carried out within the framework of the theme of state task No. 0389-2016-002 (2018–2020) and with the support of the project by UB of R AS No. 18-10-2-38.

IntechOpen

IntechOpen

Author details

Vladimir Osipov*, Vyacheslav Platonov, Vladislav Shitov and Vladimir Solomonov
Institute of Electrophysics of Ural Division of RAS, Yekaterinburg, Russia

*Address all correspondence to: osipov@iep.uran.ru

IntechOpen

© 2020 The Author(s). Licensee IntechOpen. This chapter is distributed under the terms of the Creative Commons Attribution License (http://creativecommons.org/licenses/by/3.0), which permits unrestricted use, distribution, and reproduction in any medium, provided the original work is properly cited. CC BY

References

[1] Steen WM. 1 - 'Light' industry: an introduction to laser processing and its industrial applications. In: Lawrence J, Pou J, Low DKY, Toyserkani E, editors. Handbook of Woodhead Publishing Series in Welding and Other Joining Technologies, Advances in Laser Materials Processing. Woodhead Publishing; 2010. pp. 3-19. DOI: 10.1533/9781845699819.1.3

[2] Richardson M. Laser materials processing technologies and the future. In: Proceedings of the Conference on Lasers and Electro-Optics (CLEO Pacific Rim), 24-28 August 2015; Busan, South Korea. Paper 25D3-1

[3] Malinauskas M, Žukauskas A, Hasegawa S, Hayasaki Y, Mizeikis V, Buividas R, et al. Ultrafast laser processing of materials: from science to industry. Light Sci Appl. 2016 Aug 12;**5**(8):e16133. DOI: 10.1038/lsa.2016.133

[4] Evangelista B, NIF experiments draw interest at APS conference [Internet]. 2019. Available from: http://www.llnl.gov/news/nif-experiments-draw-interest-aps-conference [Accessed: 2020-09-29]

[5] Ribeyre X, Schurtz G, Lafon M, Galera S, Weber S. Shock ignition: an alternative scheme for HiPER. Plasma Physics and Controlled Fusion. 2009;**51**(1):015013. DOI: 10.1088/0741-3335/51/1/015013

[6] Arzeno H. Premier tir le 2 décembre au Laser Megajoule [Internet]. 2014. Available from http://www.sudouest.fr/2014/01/11/premier-tir-le-2-decembre-au-laser-megajoule-1425695-2941.php [Accessed: 2020-09-29]

[7] Ikesue A, Kinoshita T, Kamata K, Yoshida K. Fabrication and optical properties of high-performance polycrystalline Nd: YAG ceramics for solid-state lasers. Journal of the American Ceramic Society. 1995;**78**(4):1033-1040. DOI: 10.1111/j.1151-2916.1995.tb08433.x

[8] Ikesue A, Aung YL, Lupei V. Ceramic lasers. Cambridge, UK: Cambridge University Press; 2013 445 p

[9] Ikesue A, Aung YL. Synthesis of Yb:YAG ceramics without sintering additives and their performance. Journal of the American Ceramic Society. 2017;**100**:26-30. DOI: 10.1111/jace.14588

[10] Latham WP, Lobad A, Newell TC, Stalna KD, Phipps C. 6.5 kW, Yb:YAG ceramic thin disk laser. AIP Conf. Proc. 2010;**1278**:758-764. DOI: 10.1063/1.3507169

[11] Peng YH, Cheng J, Cheah YY, Lai K, Lau E, Ang S. High brightness continuous wave ceramic Yb:LuAG thin-disk laser. Optics Express. 2015;**23**:19618-19623. DOI: 10.1364/OE.23.019618

[12] Liu W, Li J, Jiang B, Zhang D, Pan Y. 2.44 kW laser output of Nd:YAG ceramic slab fabricated by a solid-state reactive sintering. Journal of Alloys and Compounds. 2012;**538**:258-261. DOI: 10.1016/j.jallcom.2012.05.050

[13] Chen J, Li J, Xu J. Liu W, Bo Y, Feng X, et. al. 4350 W quasi-continuous-wave operation of a diode face-pumped ceramic Nd: YAG slab laser. Optics & Laser Technology. 2014;63:50-53. DOI: 10.1016/j.optlastec.2014.03.005

[14] Yamamoto RM, Bhachu BS, Cutter KP, Fochs SN, Letts SA, Parks CW, Rotter MD, Soules TF. The use of large transparent ceramics in a high powered, diode pumped solid state laser. In Proceedings of Conference on Advanced Solid-State. Photonics. 27-30 January 2008; Nara, Japan. Paper WC5.

[15] Northrop Grumman Scales New Heights in Electric Laser Power, Achieves 100 Kilowatts From a Solid-State Laser [Internet]. 2018. Available from: http://news.northropgrumman.com/news/releases/photo-release-northrop-grumman-scales-new-heights-in-electric-laser-power-achieves-100-kilowatts-from-a-solid-state-laser. [Accessed: 2020-09-29]

[16] Mason P, Divoký M, Ertel K, Pilař J, Butcher T, Hanuš M, et al. Kilowatt average power 100 J-level diode pumped solid state laser. Optica. 2017;**4**(4):438-439. DOI: 10.1364/OPTICA.4.000438

[17] Tokurakawa M, Takaichi K, Shirakawa A, Ueda K, Yagi H, Yanagitani T, et al. Diode-pumped 188 fs mode-locked Yb^{3+}:Y_2O_3 ceramic laser. Applied Physics Letters. 2007;**90**. DOI: 071101(3), 10.1063/1.2476385

[18] Endo M, Ito I, Kobayashi Y. Direct 15-GHz mode-spacing optical frequency comb with a Kerr-lens mode-locked Yb:Y_2O_3 ceramic laser. Optics Express. 2015;**23**(2):1276-1282. DOI: 10.1364/OE.23.001276

[19] Tokurakawa M, Shirakawa A, Ueda K, Yagi H, Noriyuki M, Yanagitani T, et al. Diode-pumped ultrashort-pulse generation based on Yb^{3+}:Sc_2O_3 and Yb^{3+}:Y_2O_3 ceramic multi-gain-media oscillator. Optics Express. 2009;**17**(5):3353-3361. DOI: 10.1364/OE.17.003353

[20] Kagan MA, Khazanov EA. Compensation for thermally induced birefringence in polycrystalline ceramic active elements. Quantum Electronics. 2003;**33**(10):876-882. DOI: 10.1070/QE2003v033n10ABEH002516

[21] An L, Ito A, Goto T. Effect of sintering temperature on the transparency and mechanical properties of lutetium aluminum garnet fabricated by spark plasma sintering. Journal of the European Ceramic Society. 2012;**32**(12):3097-3102. DOI: 10.1016/j.jeurceramsoc.2012.04.020

[22] Kijko VS, Maksimov RN, Shitov VA, Demakov SL, Yurovskikh AS. Sintering of transparent Yb-doped Lu_2O_3 ceramics using nanopowder produced by laser ablation method. Journal of Alloys and Compounds. 2015;**643**:207-211. DOI: 10.1016/j.jallcom.2015.04.127

[23] Sokol M, Kalabukhov S, Kasiyan V, Dariel MP, Frage N. Functional Properties of Nd:YAG polycrystalline ceramics processed by high-pressure spark plasma sintering (HPSPS). Journal of the American Ceramic Society. 2016;**99**:802-807. DOI: 10.1111/jace.14051

[24] Zhang W, Lu T, Ma B, Wei N, Lu Z, Li F, et al. Improvement of optical properties of Nd:YAG transparent ceramics by post-annealing and post hot isostatic pressing. Optical Materials. 2013;**35**(12):2405-2410. DOI: 10.1016/j.optmat.2013.06.042

[25] Yang Zhang Y, Cai M, Jiang B, Fan J, Zhou C, Mao X, et al. Micro-structure of grain boundary in post-annealed sinter plus HIPed Nd:$Lu_3Al_5O_{12}$ ceramics. Optical Materials Express. 2014;**4**:2182-2189. DOI: 10.1364/OME.4.002182

[26] Chrétien L, Boulesteix R, Maître A, Sallé C, Reignoux Y. Post-sintering treatment of neodymium-doped yttrium aluminum garnet (Nd:YAG) transparent ceramics. Optical Materials Express. 2014;**4**:2166-2173. DOI: 10.1364/OME.4.002166

[27] Osipov VV, Solomonov VI, Orlov AN, Shitov VA, Maksimov RN, Spirina AV. Characteristics of yttrium oxide laser ceramics with additives. Quantum Electronics. 2013;**43**(3):276-281. DOI: 10.1070/QE2013v043n03ABEH015029

[28] Osipov VV, Kotov YuA, Ivanov MG, Samatov OM, Lisenkov VV,

Platonov VV, Murzakaev AM, Medvedev AI, Azarkevich EI. Laser synthesis of nanopowders. Laser Physics. 2006;16(1):116-120. DOI: 10.1117/12.633667

[29] Osipov VV, Platonov VV, Lisenkov VV. Laser ablation synthesis and properties of nanocrystalline oxide powders. in Handbook of Nanoparticles, ed.: Aliofkhazraei M, Springer International Publishing Switzerland. 2015. 1376 p. DOI 10.1007/978-3-319-13188-7_8-1.

[30] Osipov VV, Platonov VV, Lisenkov VV. Laser ablation plume dynamics in nanoparticle synthesis. Quantum Electronics. 2009;**39**(6):541-546. DOI: 10.1070/QE2009v039n06ABEH013981

[31] Osipov VV, Solomonov VI, Platonov VV, Snigireva OA, Ivanov MG, Lisenkov VV. Laser plume spectroscopy. 2. Graphite and yttrium-stabilized zirconium oxide targets. Quantum Electronics. 2005;**36**(7):633-637. DOI: 10.1070/QE2005v035n07ABEH004087

[32] Osipov VV, Lisenkov VV, Platonov VV, Orlov AN, Podkin AV, Savvin IA. Effect of pulses from a high-power ytterbium fiber laser on a material with a nonuniform refractive index. I. Irradiation of yttrium oxide targets. Technical Physics. 2014;**59**(5):716-723. DOI: 10.1134/S1063784214050223

[33] Platonov VV, Kochurin EA, Osipov VV, Lisenkov VV, Zubarev NM. Characteristic properties of laser ablation of translucent targets. Laser Physics. 2018;**28**(7). DOI: 076002 (8pp), 10.1088/1555-6611/aabdb4

[34] Osipov VV, Platonov VV, Lisenkov VV, Tikhonov EV, Podkin AV. Study of nanoparticle production from yttrium oxide by pulse-periodic radiation of ytterbium fiber laser. Applied Physics A. 2018;**124**:3. DOI: 10.1007/s00339-017-1348-9

[35] Osipov VV, Solomonov VI, Shitov VA, Maksimov RN, Orlov AN, Murzakaev AM. Optical ceramics based on yttrium oxide doped with tetravalent ions. Russian Physics Journal. 2015;**58**:107-116. DOI: 10.1007/s11182-015-0469-x

[36] Boltachev GSh, Lukyashin KE, Shitov VA, Volkov NB. Threedimensional simulations of nanopowder compaction processes by granular dynamics method. Physical Review E. 2013;88(1):012209(1-12). DOI: 10.1103/PhysRevE.88.012209

[37] Osipov VV, Khasanov OL, Shitov VA, Dvilis ES, Ivanov MG, et al. Optical $Nd^{3+}Y_2O_3$ ceramics of nanopowders compacted by static pressure using the ultrasonic method. Nanotechnologies in Russia. 2008;**3**(7-8):474-480. DOI: 10.1134/S199507800807010045.

[38] Boltachev GS, Volkov NB. Size effect in nanopowder compaction. Technical Physics Letters. 2010;**36**:823-826. DOI: 10.1134/S1063785010090142

[39] Sato Y, Saikawa J, Taira T, Ikesue A. Characteristics of Nd^{3+}-doped $Y_3ScAl_4O_{12}$ ceramic laser. Optical Materials. 2007;**29**(10):1277-1282. DOI: 10.1016/j.optmat.2006.01.032

[40] Ma J, Wang J, Shen D, Ikesue A, Tang D. Generation of sub-100-fs pulses from a diode-pumped Yb:$Y_3ScAl_4O_{12}$ ceramic laser. Chinese Optics Letters. 2017;**15**(12):121403. DOI: 10.3788/COL201715.121403

[41] Greskovich C, Chernoch JP. Polycrystalline ceramic lasers. Journal of Applied Physics. 1973;**44**(10):4599-4606. DOI: 10.1063/1.1662008

[42] Bagayev SN, Osipov VV, Pestryakov EV, Solomonov VI, Shitov VA, Maksimov RN, et al. Laser ceramics with disordered crystalline structure. Journal of Appl. Mechanics

and Technical Physics. 2015;**56**(1):150-157. DOI: 10.1134/S0021894415010228

[43] Osipov VV, Solomonov VI, Orlov AN, Shitov VA, Maksimov RN, Spirina AV. Characteristics of yttrium oxide laser ceramics with additives. Quantum Electronics. 2013;**43**(3):276-281. DOI: 10.1070/QE2013v043n03ABEH015029

[44] Solomonov VI, Spirina AV, Konev SF, Cholach SO. Trivalent zirconium and hafnium ions in yttrium oxide ceramics. Optics and Spectroscopy. 2014;**116**(5):793-797. DOI: 10.1134/S0030400X14050257

[45] Toci G, Pirri A, Patrizi B, Maksimov RN, Osipov VV, Shitov VA, et al. High efficiency emission of a laser based on Yb-doped $(Lu,Y)_2O_3$ ceramic. Optical Materials. 2018;**83**:182-186. DOI: 10.1016/j.optmat.2018.06.006

[46] Wang SF, Zhang J, Luo DW, Gu F, Tang DY, Dong ZL, et al. Transparent ceramics: Processing, materials and applications. Progress in Solid State Chemistry. 2013;**41**(1-2):20-54. DOI: 10.1016/j.progsolidstchem.2012.12.002

[47] Li Y, Zhou S, Lin H, Hou X, Li W, Teng H, et al. Fabrication of Nd:YAG transparent ceramics with TEOS, MgO and compound additives as sintering aids. Journal of Alloys and Compounds. 2010;**502**(1):225-230. DOI: 10.1016/j.jallcom.2010.04.151

[48] Bagayev SN, Osipov VV, Solomonov VI, Shitov VA, Maksimov RN, Lukyashin KE, et al. Fabrication of Nd^{3+}:YAG laser ceramics with various approaches. Optical Materials. 2012;**34**(8):1482-1487. DOI: 10.1016/j.optmat.2012.03.004

[49] Osipov VV, Shitov VA, Solomonov VI, Lukyashin KE, Spirina AV, Maksimov RN. Composite Nd:YAG/Cr^{4+}:YAG transparent ceramics for thin disk lasers. Ceramics International. 2015;**41**(10):13277-13280. DOI: 10.1016/j.ceramint.2015.07.109

[50] Osipov VV, Maksimov RN, Shitov VA, Lukyashin KE, Toci G, Vannini M, et al. Fabrication, optical properties and laser outputs of Nd:YAG ceramics based on laser ablated and pre-calcined powders. Optical Materials. 2017;**71**:45-49. DOI: 10.1016/j.optmat.2016.06.021